ELSEVIER

Chemical Engineering Journal 136 (2008) 358–363

Chemical Engineering Journal

www.elsevier.com/locate/cej

Application of Anderson–Schulz–Flory (ASF) equation in the product distribution of slurry phase FT synthesis with nanosized iron catalysts

Akram Tavakoli, Morteza Sohrabi *, Ali Kargari

Amirkabir University of Technology, Faculty of Chemical Engineering, Tehran 15914, Iran

Received 2 October 2006; received in revised form 11 April 2007; accepted 13 April 2007

Abstract

Application of ASF equation on the product distribution of FT synthesis using nanosized iron catalysts is studied. The dependencies of product distribution on the reaction temperature and reduction conditions of nanocatalysts are investigated by the growth probability of hydrocarbons (α). The latter has been calculated for three different FT catalysts under various operating conditions and hydrocarbon ranges (n). Since ASF equation may not be suitable for these systems, a new approach has been put forward. According to such an approach the molar product distribution is applied to calculate α values from the slopes of the plots of ln (mol.%/n) against n. The latter are called the quasi-ASF plots. Quasi-ASF plots follow the same trends as those of ASF but with an improved linearity.

Keywords: Anderson–Schulz–Flory; FT synthesis; Nanosized iron catalysts

1. Introduction

Fischer–Tropsch (FT) synthesis discovered in 1920s remains one of the major research topics within alternate fuels R&D [1]. FT reaction is the catalytic hydrogenation of carbon monoxide which yields a wide range of alkenes, alkanes, and oxygenated compounds (aldehydes, alchohols, ketones, and acids) [2].

The interest in FT synthesis is multi-folds: (1) it is one of the leading gas-to-liquid (GTL) options to transport stranded natural gas, (2) it directly yields hydrocarbon-based transportation fuels, (3) the produced hydrocarbon fuels are of high quality due to a very low aromaticity and low in sulfur as well as other impurities and, as such, are classified as clean fuels, and (4) potentially lower price of FT crude oil compared to that of the steadily diminishing world supply of petroleum, makes the FT reaction as a favorable process [3–6].

Two classes of reactors are used in the FT process: fixed and fluidized beds. The latter can be subdivided into two-phase (solid and gas) and three-phase (solid, liquid, and gas) or slurry systems. Among these types of reactors, the slurry three-phase catalytic reactor seems to be a better choice due to the efficient temperature control, lower pressure drop compared to the fixed bed reactors, on-line removal/addition of catalyst that allows longer reactor runs at higher average conversions, smaller catalysts particles which avoid intraparticle diffusion effects and deposition of heavy product on the catalyst. In addition, it is best suited to study the dependence of product selectivity on the concentrations of carbon monoxide, hydrogen and alkenes [2,7,8].

Only the four members of the group VIII (Fe, Co, Ni, and Ru) have sufficiently high activities for the hydrogenation of carbon monoxide to warrant their use as effective FT catalysts. Among the four metals, ruthenium is the most active. The cost of ruthenium is, however, prohibitively high relative to the other metals and furthermore the worldwide amount of available Ru is hardly sufficient for one large FT plant. Nickel is also very active but has two major drawbacks. Being a powerful hydrogenating catalyst it produces less of the high value alkenes and more the low value methane than Co or Fe catalysts. At the temperatures and pressures at which the FT plants operate, nickel forms volatile carbonyls, results in continuous loss of metal from the FT reactors. From what was mentioned above it is clear that only cobalt and iron-based catalysts may be considered as practical FT catalysts [2]. Iron-based catalyst systems remain the preferred choice

* Corresponding author. Tel.: +982164543155; fax: +982166405847.
E-mail address: sohrabi@aut.ac.ir (M. Sohrabi).

1385-8947/$ – see front matter © 2007 Elsevier B.V. All rights reserved.
doi:10.1016/j.cej.2007.04.017

in commercial FT synthesis plants due to their low cost and their propensity to yield high olefinic content in the hydrocarbon distribution [1,9]. But it is well known that low space-time-yield (STY), low product selectivity, catalyst agglomeration and sintering, limit the use of Fe-based catalysts that operate between 533 and 573 K [1,10]. Although cobalt is more costly than iron, supported cobalt is valued as a FT catalyst because of its stability, high activity, and low yield of oxygenated products [6].

Studies with highly dispersed metals as nanocatalysts are of interest because nanosizing increases surface area that exposes more catalytic sites, the use of nanosized metals could potentially enhance activity of heterogeneous catalysts that dominate the field of catalysis [3,4,11]. In addition, in exothermic reactions such as CO hydrogenation, nanocatalysts are likely to be more effective and selective or show other interesting properties as the temperature is lowered. For example, it has been reported that FT synthesis could be achieved at a lower temperature of 493 K with nanosized particles of Fe in slurry phase. In this case, the water–gas shift (WGS) activity is ceased and no CO_2 is produced during FT synthesis [3,4].

The molecular mass spread of the FT products can be varied over a wide range by changing the operating conditions and/or the type of catalyst [2,7,12]. There is always a clear inter-relationship between the various FT products. These inter-relationships are due to the step-wise growth nature of the FT mechanism [2,7]. The details of the FT reaction on a molecular level still remain a controversial matter, nevertheless, in all proposed mechanisms a step-wise growth procedure is assumed. It is often stated that knowledge of the actual mechanism of the FT reactions occurring on the catalyst surface will lead to improvements in the process [2].

If the hydrocarbon chain is formed step-wise by insertion or addition of C_1 intermediates with constant growth probability (α) then the chain length distribution is given by the Anderson–Schulz–Flory (ASF) distribution [7]. Assuming that α to be independent from hydrocarbon chain length, an equation may be derived as follows,

$$\log\left(\frac{W_n}{n}\right) = n\log\alpha + \text{const.} \quad (1)$$

where W_n is the mass fraction of the species with carbon number n. From the slope of the plot of log (W_n/n) against n the value of α is obtained [2]. The majority of the reported ASF plots showed a nearly straight-line only in the C_4–C_{12} region. A number of authors have determined the growth factor from the straight-line portion of the ASF plot. This made the experimental determination of α somehow arbitrary [13].

However, for most iron, cobalt and ruthenium catalysts marked deviations from this ideal distribution are observed [2,7,13]. In these cases, product distributions can be represented by superposition of two ASF distributions. This bimodal distribution was interpreted by different phenomena [7,13–15]. The product distribution of FT synthesis in bimodal distribution has been characterized by two independent ASF distributions with different chain growth probabilities (α_1, α_2) and the point of intersection of the two ASF distributions. The fraction of methane in total products does not obey the ASF equation due to the several routes of formation. Furthermore, ethene can either start or can be incorporated into growing chains. Therefore, the determination of growth probabilities α_1 and α_2 of the bimodal ASF distribution is based on hydrocarbons with carbon numbers greater than two [7].

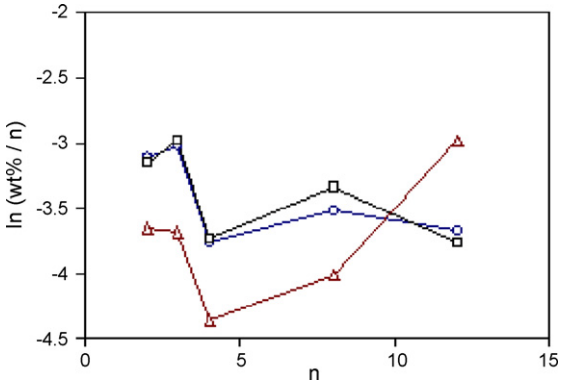

Fig. 1. ASF plot of the hydrocarbon distribution obtained during FT synthesis catalyzed by NANOCAT (◯), BASF (□) and UCI (△) catalysts. Reaction conditions: catalyst precursor loading = 4.6 wt.%; solvent: ethylflopolyolefin-164 = 330 g; synthesis gas: $H_2/CO = 66\%/34\%$; $P = 0.78$ MPa; GHSV = 4.6 NL/(g Fe h); $T = 513$ K; run time = 120 h. The initial oxide catalyst precursor was initially reduced with CO at 553 K in all three cases.

Since the selectivity spectrum appears to be determined largely by the α values, the control of selectivity will be determined by those factors that influence the latter. These variables consist of temperature, catalyst type and promoters, gas composition and partial pressures inside the catalyst bed [2,7,14]. Literature reports indicate that the value of the growth factor decreases with increasing temperature, and increasing H_2/CO ratio [13].

Calculations have demonstrated that if the range of the assumed values for α is narrow, a single α can adequately describe the molecular weight distribution. The deviations from an ideal ASF distribution are so little, that they cannot be convincingly detected with available analytical accuracies. If the assumed α ranges were wide, the calculated ASF plots showed smooth curving "positive deviations", exhibiting increasing curvature with increasing assumed α ranges [13] as shown in Fig. 1.

The aim of the present study is to investigate the application of ASF equation in the product distribution of FT synthesis with nanosized iron catalysts. Furthermore, the dependencies of product distribution on the reaction temperature and reduction conditions of nanocatalysts were also investigated. Since there are only a few reports available in the literature specifically related to the slurry phase FT products distribution using nanosized catalysts, the data reported by Mahajan et al. [3,4] have applied in this study.

Table 1 shows the data summary of FT synthesis runs catalyzed by unsupported nano-Fe particles (NANOCAT and BASF) and supported UCI systems [3].

To consider the effects of different reduction conditions on product distribution, the ASF plots were drawn for CO- and syngas-treated NANOCAT catalysts (Fig. 2). Similar to the previous case, C_1 fraction was ignored. The upward shift in the ASF

Table 1
Data summary of FT synthesis runs[a] catalyzed by unsupported nano-Fe particles (NANOCAT and BASF) and supported UCI systems [3]

	NANOCAT			BASF	UCI
	513 K	533 K[b]	533 K[c]	513 K	513 K
% conversion					
H_2	34.8	44.7	14.3	41.7	38.7
CO	42.9	52.1	16.2	55.9	65.4
$H_2 + CO$	40.5	46.8	14.9	48.5	47.4
Hydrocarbons product distribution (wt.%)					
C_1	12.8	16.0	16.4	10.7	7.0
C_2	8.9	11.2	11.4	8.5	5.2
C_3	14.6	15.4	13.8	15.2	0.6
C_4	9.3	11.4	8.8	9.6	5.1
C_5–C_{10}	23.7	30.0	23.0	28.2	14.5
C_{11+}	30.7	16.0	29.6	27.8	60.6
Overall product distribution (wt.%)					
Hydrocarbon	31.8	32.3	35.9	30.5	28.4
H_2O	36.5	37.2	40.6	30.5	25.0
CO_2	31.7	30.5	23.5	39.0	46.6
STY (kg/(kg Fe h))					
C_1–C_4	0.26	0.37	0.09	0.36	0.22
C_{5+}	0.14	0.17	0.04	0.20	0.16

[a] Reaction conditions: catalyst loading = 4.6 wt.%; solvent: ethylflopolyolefin-164 = 330 g; synthesis gas: $H_2/CO = 66\%/34\%$; $P = 0.78$ MPa; $V = 4.5$–4.7 NL/(g Fe h); run time = 120 h. The initial oxide catalyst precursor was initially reduced with CO at 553 K in all cases.
[b] At $P = 2.77$ MPa; SV = 5.78 NL/(g Fe h).
[c] Initially reduced with $67\%H_2/33\%CO$ gas mixture. Syngas feed rates during FT synthesis were 6.3 (24 h) and 4.4 (28 h) NL/(g Fe h). Total run time = 52.5 h. Operating $P = 2.8$ MPa.

plot of CO-treated NANOCAT catalyst, particularly in case of C_2–C_8 range, may demonstrate the higher activity of this catalyst relative to that of syngas-treated catalyst. The calculated α and R^2, regression coefficient, values in Table 2 showed that the correlation between CO-treated NANOCAT catalyst and ASF equation is better than that of syngas-treated catalyst and ASF relation. The larger values for α determined in the present study relative to those reported in the literatures [3,4] may be either related to the narrow hydrocarbon range with small n applied in this study, or to the less applicability of ASF equation for these systems.

Table 2
Calculated growth probabilities and R^2 values in different conditions

	Wt.%		Mol.%	
	α	R^2	α	R^2
$T = 513$K				
NANOCAT	0.9516	0.3846	0.8060	0.8597
BASF	0.9484	0.4026	0.8033	0.8836
UCI	1.0703	0.3054	0.9065	0.3426
Reduction conditions				
CO-treated NANOCAT	0.8861	0.7545	0.7504	0.9363
Syngas-treated NANOCAT	0.9292	0.4937	0.7870	0.8459
Reaction temperatures				
$T = 513$ K (NANOCAT)	0.9516	0.3846	0.8060	0.8597
$T = 533$ K (NANOCAT)	0.8861	0.7545	0.7504	0.9363

Another parameter that can affect the product distribution is reaction temperature. ASF plots for NANOCAT catalysts at various reaction temperatures and under different operating conditions are shown in Fig. 3. It is clear from this figure that, with increase in reaction temperature the hydrocarbon products within C_1–C_8 range are also increased. The calculated α and R^2 values with C_1 fraction ignored are shown in Table 2. It is evident that ASF distribution is more accurate within higher reaction temperatures. This may indicate that the step-wise mechanism is predominant at higher reaction temperatures.

In all states mentioned above, it may be observed that ASF plots are not linear, which in turn reflect the dependency of α values on carbon numbers. In order to examine the accuracy of ASF equation for FT product distribution on nanosized iron catalysts, values for α were calculated at different carbon number ranges. To consider variation of α with the range of hydrocarbon, average values for α ($\bar{\alpha}$), α range width, and standard deviation for different α series in each individual catalyst were calculated and are presented in Table 3. It is evident that α values are widely scattered and R^2 values are so small that the application of ASF equation for FT product distribution have to be approached with cautious.

To resolve the anomaly, the molar product distribution was considered in the quasi-ASF plots. The latter is in fact a plot of ln (mol.%/n) against carbon number. Quasi-ASF plot were drawn for different catalysts (Fig. 4), CO- and syngas-treated

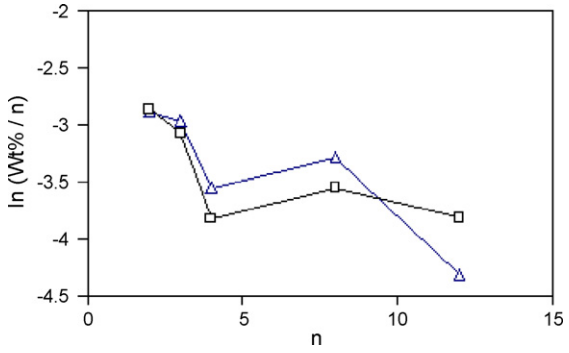

Fig. 2. ASF plot of the hydrocarbon distribution obtained during FT synthesis catalyzed by NANOCAT. The initial oxide catalyst precursor was initially reduced with CO (△), and syngas (□). Other reaction conditions are as Table 1.

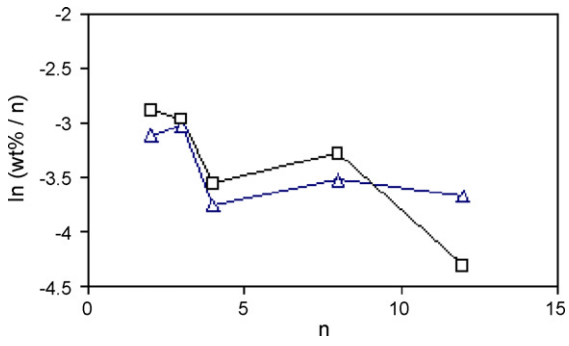

Fig. 3. ASF plot of the hydrocarbon distribution obtained during FT synthesis catalyzed by NANOCAT at two reaction temperatures. $T = 513$ K (△), and $T = 533$ K (□).

Table 3
Calculated growth probabilities and R^2 values in different carbon ranges

n	wt. (%)						Mol.%					
	NANOCAT		BASF		UCI		NANOCAT		BASF		UCI	
	α	R^2	α	R^2	α	R^2	α	R^2	α	R^2	α	R^2
2–3	1.09	1.00	1.19	1.00	0.97	1.00	0.75	1.00	0.81	1.00	0.66	1.00
2–4	0.72	0.65	0.75	0.54	0.70	0.78	0.52	0.91	0.54	0.87	0.50	0.95
2–8	0.93	0.29	1.04	0.09	0.95	0.19	0.75	0.81	0.78	0.76	0.77	0.77
2–12	0.95	0.39	0.95	0.40	1.07	0.31	0.81	0.86	0.80	0.88	0.91	0.34
dα[a]	0.371		0.441		0.370		0.286		0.272		0.403	
$\bar{\alpha}$	0.925		0.983		0.923		0.707		0.734		0.710	
S[b]	0.070		0.102		0.074		0.049		0.051		0.087	

[a] α range width = max α − min α.
[b] $S = \sum_i (\alpha_i - \bar{\alpha})^2$.

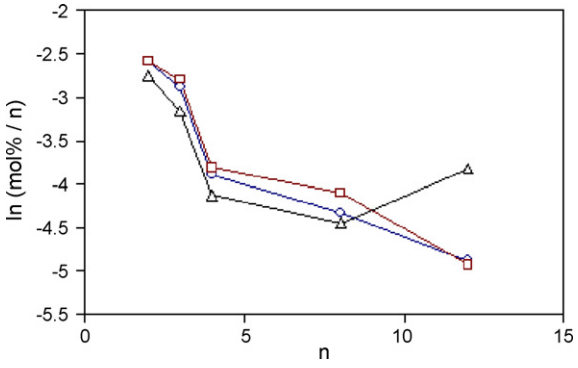

Fig. 4. Quasi-ASF plot of the hydrocarbon distribution obtained during FT synthesis catalyzed by NANOCAT (◯), BASF (□) and UCI (△) catalysts. Reaction conditions: catalyst precursor loading = 4.6 wt.%; solvent: ethylflopolyolefin-164 = 330 g; synthesis gas: $H_2/CO = 66\%/34\%$; $P = 0.78$ MPa; GHSV = 4.6 NL/(g Fe h); $T = 513$ K; run time = 120 h. The oxide catalyst precursor was initially reduced with CO at 553 K in all three cases.

NANOCAT catalysts (Fig. 5), and different reaction temperatures (Fig. 6). The trends of these plots are similar to those of ASF plots, however, with improved linearity. In other words, the quasi-ASF plots can explain the qualitative efficiency of each catalyst similar to ASF; however, the use of molar product distribution in calculation of α may be more accurate (see Table 2). The data in Table 3 show that the deviations of α values from average values determined from quasi-ASF plots are smaller than those calculated using conventional technique. In addition with quasi-ASF approach, the α range width obtained is narrower, the average values for α are closer to those stated in the literature [3,4] and the number of data required is less than those used in ASF calculation.

Fig. 7 shows the α value variation as a function of cumulative product distribution on wt.% and mol.% basis. These plots demonstrated that the growth chain probability at certain wt.% and/or mol.% of products is largest for UCI catalyst. This means that the deactivation of UCI catalyst compared to two other catalysts is slower. It is in good agreement with Mahajan et al. data [3,4] for CO and H_2 conversions after 120 h which were 43 and 35% for NANOCAT, 55 and 42% for BASF and, 64 and 37% for UCI, respectively. The faster rate of deactivation of nanocatalysts is understandable due to their larger surface/volume ratios. It is also evident from this figure that α values are increased by increasing the conversion. This may be an indication of a broad product distribution.

The ASF and quasi-ASF plots were also drawn for Fe-HZSM5 bifunctional catalyst in a fixed bed reactor under different reaction conditions as shown in Figs. 8 and 9, respectively. These figures may confirm concepts presented previously. Namely, both quasi-ASF and ASF graphs follow similar

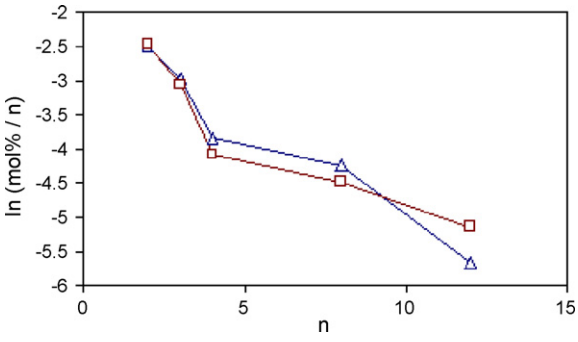

Fig. 5. Quasi-ASF plot of the hydrocarbon distribution obtained during FT synthesis catalyzed by NANOCAT. The oxide catalyst precursor was initially reduced with CO (△), and syngas (□). Other reaction conditions are as Table 1.

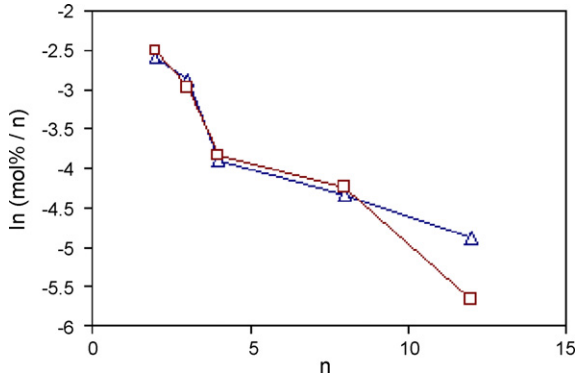

Fig. 6. Quasi-ASF plot of the hydrocarbon distribution obtained during FT synthesis catalyzed by NANOCAT at different reaction temperatures. $T = 513$ K (△), and T = 533K (△).

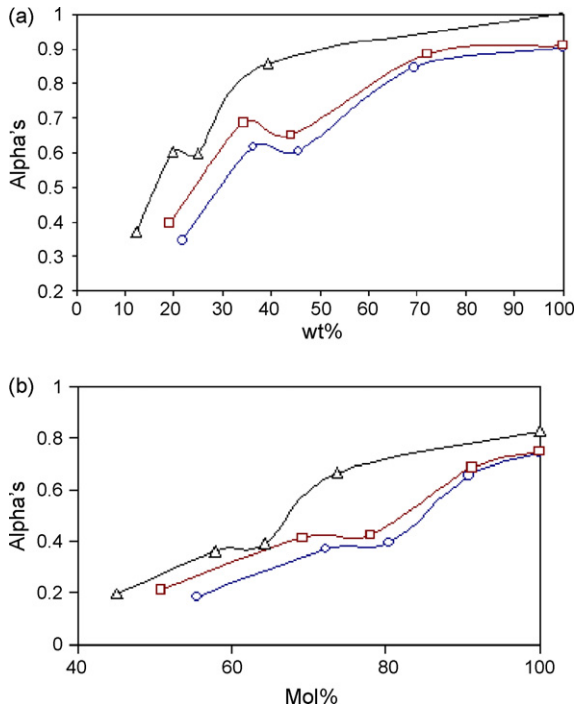

Fig. 7. The α values variations as a function of cumulative product distribution based on wt.% (a) and based on mol.% (b). NANOCAT (◯), BASF (□), UCI (△).

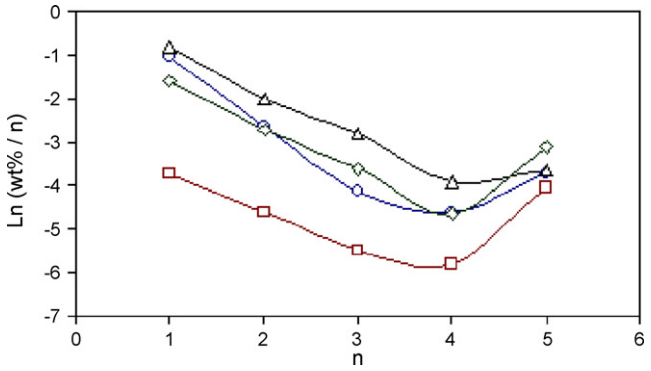

Fig. 8. ASF plots for Fe-HZSM5 bifunctional catalyst in a fixed bed reactor. Run numbers: 2 (◯), 3 (□), 8 (△), and 10 (◊). Reaction conditions are as ref. [16].

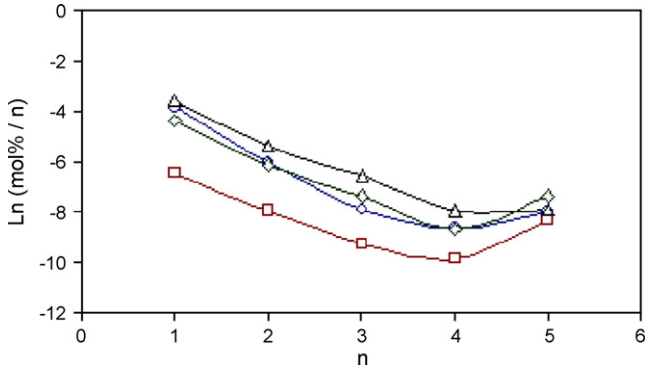

Fig. 9. Quasi-ASF plots for Fe-HZSM5 bifunctional catalyst in a fixed bed reactor. Run numbers: 2 (◯), 3 (□), 8 (△), and 10 (◊). Reaction conditions are as ref. [16].

trends; however the quasi-ASF plots have higher regression coefficients.

2. Conclusion

Since the experimental determination of α is somewhat arbitrary, the calculation of this parameter has been performed at different hydrocarbon numbers as proposed in the literatures. In a particular study the C_1 fraction was considered, while in another case C_2 and C_8 fractions were ignored. In performing the calculations, C_5–C_{10} and C_{11+} ranges were taken as C_8 and C_{12} hydrocarbons, respectively. In all cases considered in the present investigation it was observed that by application of mol.% instead of wt.% data, the results obtained were more reasonable, i.e., narrower α range width, meaningful $\bar{\alpha}$, higher regression coefficients, and smaller standard deviation. Furthermore, calculations with nanocatalysts based on mol.% led to highly reasonable results when C_1 fraction was ignored, while in case of wt.% data the results were not stable. In other words, in certain cases satisfactory results obtained for α when C_1 fraction was considered, such as syngas-treated NANOCAT catalyst, while in some other circumstances reasonable results were found by ignoring C_2 and C_8 fractions, such as CO-treated NANOCAT catalyst. Dependency of α values on hydrocarbon numbers is noteworthy and shows that ASF equation may be not suitable for nanoparticle catalyst systems and may indicate that different growth mechanisms may be dominant during hydrocarbon synthesis with nanocatalysts. Another advantage of molar calculation is the need for less hydrocarbon ranges data while the results of such calculations are close to α values based on mass% calculations, obtained in some previous studies [3,4] by taking into account some large ranges of hydrocarbons data.

Referring to Figs. 1 and 7 and Table 3, it may be observed that the BASF catalyst for FT process seems to be more active in comparison with that of UCI. In addition, the BASF catalyst's stability is higher than that of NANOCAT catalyst.

References

[1] H Schulz, Appl. Catal. A 186 (1999) 3–12.
[2] Istvan T. Horvath ,(Editor in Chief), Encyclopedia of Catalysis. Mark E. Day, Fischer-Tropsch Synthesis-Industrial, vol. 3, John Wiley & Sons, 2003, pp. 347–403.
[3] D. Mahajan, P. Gutlich, J. Ensling, K. Pandya, U. Stumm, P. Vijayaraghavan, Energy Fuels 17 (2003) 1210–1221.
[4] D. Mahajan, P. Gutlich, U. Stumm, Catal. Commun. 4 (2003) 101–107.
[5] M.A. Marvast, M. Sohrabi, S. Zarrinpashne, G. Baghmisheh, Chem. Eng. Technol. 28 (1) (2005) 78–86.
[6] B.C. Dunn, D.J. Covington, P. Cole, R.J. Pugmire, H.L.C. Meuzelaar, R.D. Ernst, E.C. Heider, E.M. Eyring, Energy Fuels 18 (2004) 1519–1521.
[7] J. Patzlaff, Y. Liu, C. Graffmann, J. Gaube, Appl. Catal. A 186 (1999) 109–119.
[8] V.R. Ahon, E.F. Costa Jr., J.E.P. Monteagudo, C.E. Fontes, E.C. Biscaia Jr., P.L.C. Lage, Chem. Eng. Sci. 60 (2005) 677–694.
[9] R.L. Espinoza, A.P. Steynberg, B. Jager, A.C. Vosloo, Appl. Catal. A 186 (1999) 13–26.
[10] L.D. Mansker, Y. Jin, D.B. Bukur, A.K. Datye, Appl. Catal. A 186 (1999) 277–296.

[11] C. Burda, X. Chen, R. Narayanan, M.A El-Sayed, Chem. Rev. 105 (2005) 1025–1102.
[12] W-.D. Deckwer, R. Kokuun, E. Sanders, S. Ledakowicz, Ind. Eng. Chem. Process Des. Dev. 25 (1986) 643–649.
[13] I. Puskas, R.S. Hurlbut, Catal. Today 84 (2003) 99–109.
[14] J. Patzlaff, Y. Liu, C. Graffmann, J. Gaube, Catal. Today 71 (2002) 381–394.
[15] X. Zhan, B.H. Davis, Appl. Catal. A 236 (2002) 149–161.
[16] M.A. Marvast, Fischer-Tropsch synthesis using Fe-HZSM5 as a bifunctional catalysts: kinetic and modeling studies, Ph.D. Thesis, Amirkabir University of Technology, Tehran, Iran, 2005.